Composite Structures 94 (2012) 1420–1429

Contents lists available at SciVerse ScienceDirect

Composite Structures

journal homepage: www.elsevier.com/locate/compstruct

Predictions of viscoelastic strain rate dependent behavior of fiber-reinforced polymeric composites

B.J. Yang [a], B.R. Kim [b], H.K. Lee [a,*]

[a] Department of Civil and Environmental Engineering, Korea Advanced Institute of Science and Technology, Guseong-dong, Yuseong-gu, Daejeon 305-701, Republic of Korea
[b] Civil and Architecture Engineering Department, KEPCO Engineering & Construction Company, Inc., 2354 Yonggudaero, Giheung-gu, Yongin-si, Gyeonggi-do 446-713, Republic of Korea

ARTICLE INFO

Article history:
Available online 20 November 2011

Keywords:
Micromechanics-based viscoelastic model
Discontinuous fiber-reinforced polymeric composites
Aligned and 3D randomly oriented fibers
Strain rate sensitivity

ABSTRACT

A viscoelastic damage model for aligned and 3D randomly oriented discontinuous fiber-reinforced polymeric composites is proposed. The model, which predicts the effective viscoelastic stress–strain behavior of the composites, is based on a combination of the Laplace-transformed superposition principle and the ensemble-averaged micromechanics. The Weibull's damage function is incorporated into the model for the modeling of the evolution of damaged fibers. An inverse analysis based on experimental data is adopted to simulate the strain rate sensitivity of the model. A series of numerical simulations based on the proposed model are performed to examine the influence of damage parameters, fiber orientations, strain rates, and the aspect ratio of discontinuous fibers on the behavior of the composites. In addition, experimental comparisons are made to illustrate and assess the predictive capability of the proposed model.

1. Introduction

The damage and strain rate sensitivity of viscoelastic composites are fundamental issues for the safe application of the composites [41]. Although constitutive relations of fiber-reinforced polymeric composites have been widely studied, few studies have dealt with viscoelastic characteristics of polymeric composites and damage-based predictions [48,43]. In particular, the rate-dependent nature of polymeric composites is a significant factor in the development of a viscoelastic model since it significantly affects the behavior of the polymer matrix [37]. The overall behavior of discontinuous fiber-reinforced composites is also affected in a significant and practical manner by the damage phenomenon, aspect ratio and arrangement of the reinforcing fibers [46,26,53] and therefore these factors must be considered in the prediction of the composites.

Polymer matrix composites are viscoelastic solids simultaneously having elastic and viscosity properties [4]. To identify the viscoelastic phenomenon, researchers have developed several simple physical models, such as the Maxwell model, the Kelvin-Voight model, and the Standard Linear Solid model. The enumerated models comprise spring and damper elements, which signify the elastic and viscosity properties, respectively [11]. The models have been used in several simulations designed to predict the behavior of viscoelastic material [1,50]. Furthermore, advanced methods with additional considerations have also been developed to identify characteristics of the viscoelastic mechanism, particularly the thermodynamics-based process [45] and the finite-strain viscoelastic model [47].

A homogenization process is essential for polymeric composites that contain aligned or randomly oriented discontinuous fibers since the matrix and discontinuous fibers have different material characteristics [35]. A micromechanical method can be used to describe the overall mechanical behavior of composites in terms of a homogenized material, and this approach has been used to model heterogeneous composites in numerous studies (e.g., [18,19,21,33,29,23]. Several groups have used micromechanics-based viscoelastic modeling. For instance, [37] considered how the viscoelastic property affects the overall behavior of composites; and they used a generalized method of cells in which Laplace transformation of time-dependent material functions are coupled with a numerical time integration scheme. To determine the viscoelastic response of fiber-reinforced polymeric composites, [35] relied on a cylinder assemblage [17] and a generalized self-consistent scheme [3]. Refs. [15,16] also proposed a micromechanical model that analyzes the viscoelastic behavior with an imperfect interfacial condition for particulate and fiber-reinforced composites. Ref. [5] proposed a model based on the shear lag method [12] to predict the behavior of rubber matrix composites having randomly distributed short fibers. [2] developed an analytical model based on micromechanics to characterize loss tangents

* Corresponding author. Tel.: +82 42 350 3623.
E-mail address: leeh@kaist.ac.kr (H.K. Lee).

0263-8223/$ - see front matter © 2011 Elsevier Ltd. All rights reserved.
doi:10.1016/j.compstruct.2011.11.016

and the stiffness of the layers of fiber-reinforced composites. For a finite element simulation, [8] applied a nonlinear viscoelastic constitutive relation to calculate the time effects on a fiber cross-ply laminate. Ref. [44] proposed a finite element model based on the elastic–viscoelastic correspondence principle; they considered a square-packed array of fibers in unidirectional lamina composites. Ref. [6] used finite element modeling based on a numerical model to determine the effective damping characteristics of the viscoelastic response.

This study proposes an effective micromechanics-based viscoelastic damage model for polymeric composites containing aligned and 3D randomly oriented discontinuous fibers. The rate-dependent nature of the polymer matrix (phase 0) causes a viscoelastic response in composites; thus, the Boltzmann superposition principle [11,14] is coupled with an ensemble volume averaged method based on a micromechanical homogenization process [18,19]. An averaging process of fibers over 3D randomly orientations [30,31,48] is carried out in order to obtain the constitutive relations of randomly oriented discontinuous fiber-reinforced composites. Damage phenomena induced by interfacial debonding also have a remarkable influence on the overall behavior of composites. The perfectly bonded discontinuous fibers (phase 1) may be damaged as deformations increase, and these fibers are assumed to be completely debonded fibers which can be separately regarded as damaged fibers (phase 2). Accordingly, the Weibull statistics function [52,20,32,27], which is expressed as the current volume fraction of damaged fibers, is applied to the proposed model. In addition, the strain rate sensitivity is taken into account by carrying out an inverse analysis based on experimental data [13,7]. Numerical simulations are carried out to investigate how strain rate, fiber arrangement, damage parameters, and aspect ratio of discontinuous fibers affect the behavior of polymeric composites. Moreover, the predictions based on the proposed model and experimental data on aligned and 3D randomly oriented discontinuous fiber-reinforced polymeric composites [10,39] are compared for the purpose of assessing the potential of the present framework.

2. Effective viscoelastic/damage behavior of discontinuous fiber-reinforced polymeric composites

2.1. Effective elastic damage model for aligned fiber-reinforcement composites

The volume fraction of damaged fibers ϕ_2 at the level of the uniaxial tensile loading can be expressed as [49,54–56,20,21,25]

$$\phi_2 = \phi P_d(\bar{\sigma}_1) = \phi\left\{1 - \exp\left[-\left(\frac{\bar{\sigma}_1}{S_0}\right)^M\right]\right\} \tag{1}$$

where ϕ is the original fiber volume fraction, S_0 and M are damage parameters, and the internal stress of fibers (phase 1), denoted by $\bar{\sigma}_1$, can be obtained as [20,21,30,28]

$$\bar{\boldsymbol{\sigma}}_1 = \mathbf{C}_1 : [\mathbf{I} - \mathbf{S}\cdot(\mathbf{A}_1 + \mathbf{S})^{-1}]\cdot\left[\mathbf{I} - \sum_{r=1}^{2}\phi_r\mathbf{S}\cdot(\mathbf{A}_r + \mathbf{S})^{-1}\right]^{-1} : \bar{\boldsymbol{\epsilon}} \equiv \mathbf{U} : \bar{\boldsymbol{\epsilon}} \tag{2}$$

with

$$\mathbf{A}_r \equiv (\mathbf{C}_r - \mathbf{C}_0)^{-1}\cdot\mathbf{C}_0 \tag{3}$$

where $\mathbf{C}_r$ denotes the elasticity tensor of the r-phase and ϕ_r is the volume fraction of the r-phase, $\mathbf{I}$ is the fourth-rank identity tensor and $\mathbf{S}$ signifies the Eshelby's tensor [9] for a spheroidal inclusion [22]. The components of the positive defined fourth-rank tensor $\mathbf{U}$ are explicitly written as

$$U_{ijkl} = U_{IK}^{(1)}\delta_{ij}\delta_{kl} + U_{IJ}^{(2)}(\delta_{ik}\delta_{jl} + \delta_{il}\delta_{jk}) \tag{4}$$

where the components of the second-rank tensor $U_{IK}^{(1)}$ and $U_{IJ}^{(2)}$ are given by (cf. 43]

$$U_{IK}^{(1)} = \frac{T_{IK}^{(1)} + 2P_{II}^{(2)}T_{IK}^{(1)} - 2T_{II}^{(2)}\left(1 + 2P_{KK}^{(1)}\right)\Omega_{IK}}{\left(1 + 2P_{KK}^{(1)}\right)\left(1 + 2P_{II}^{(2)}\right)} - \sum_{n=1}^{3}\frac{T_{In}^{(1)}\Omega_{nK}}{1 + 2P_{nn}^{(2)}} \tag{5}$$

$$U_{IJ}^{(2)} = \frac{T_{IJ}^{(2)}}{1 + 2P_{IJ}^{(2)}} \tag{6}$$

with

$$T_{IK}^{(1)} = \lambda_1 - \frac{1}{\phi_1}\left(2\mu_1 L_{IK}^{(1)} - 2\lambda_1 L_{KK}^{(2)} - \sum_{n=1}^{3}\lambda_1 L_{nK}^{(1)}\right),$$
$$T_{IJ}^{(2)} = \frac{\mu_1\left(\phi_1 - 2L_{IJ}^{(2)}\right)}{\phi_1} \tag{7}$$

in which

$$\Omega_{I1} = \frac{\left\{1 + 2\left(P_{22}^{(1)} + P_{22}^{(2)}\right)\right\}P_{I1}^{(1)} - 2P_{21}^{(1)}P_{I2}^{(1)}}{1 + 2\left(1 + P_{11}^{(1)} + 2P_{11}^{(2)} - P_{12}^{(1)}P_{21}^{(1)} + P_{22}^{(1)}\right)P_{22}^{(2)} + \left(P_{11}^{(1)} + 2P_{11}^{(2)}\right)\left(1 + P_{22}^{(1)}\right)} \tag{8}$$

$$\Omega_{I2} = \Omega_{I3} = \frac{\left(1 + P_{11}^{(1)} + 2P_{11}^{(2)}\right)P_{I2}^{(1)} - P_{12}^{(1)}P_{I1}^{(1)}}{2\left(\frac{1}{2} + P_{22}^{(1)} + P_{22}^{(2)}\right)\left(1 + P_{11}^{(1)} + 2P_{11}^{(2)}\right) - 2P_{12}^{(1)}P_{21}^{(1)}} \tag{9}$$

with

$$P_{IK}^{(1)} = -\left(L_{IK}^{(1)} + L_{IK}^{(3)}\right) \quad P_{IJ}^{(2)} = -\left(L_{IJ}^{(2)} + L_{IJ}^{(4)}\right) \tag{10}$$

where λ_r and μ_r ($r = 0, 1$) are Lame constants of rth-phase, and the second-rank tensor $L_{IK}^{(1)}$, $L_{IJ}^{(2)}$, $L_{IK}^{(3)}$, and $L_{IJ}^{(4)}$ are given in the Appendix A.

The effective elasticity tensor $\mathbf{C}^*$ for discontinuous fiber-reinforced composites can be derived by using the ensemble-averaged volume method as [18,19]

$$\mathbf{C}^* = \mathbf{C}_0\left[\mathbf{I} + \sum_{r=1}^{2}\left\{\phi_r(\mathbf{A}_r + \mathbf{S})^{-1}\cdot[\mathbf{I} - \phi_r\mathbf{S}\cdot(\mathbf{A}_r + \mathbf{S})^{-1}]^{-1}\right\}\right] = C_{IK}^{(1)}\delta_{ij}\delta_{kl} + C_{IJ}^{(2)}(\delta_{ik}\delta_{jl} + \delta_{il}\delta_{jk}) \tag{11}$$

in which

$$C_{IK}^{(1)} = 2(\mu_0\psi_{IK}^{(1)} + \lambda_0\psi_{KK}^{(2)}) + \sum_{n=1}^{2}\lambda_0\psi_{nK}^{(1)}, \quad C_{IJ}^{(2)} = 2\mu_0\psi_{IJ}^{(2)} \tag{12}$$

with

$$\psi_{IK}^{(1)} = \Gamma_{IK}^{(1)} + \Gamma_{IK}^{(3)}, \quad \psi_{IJ}^{(2)} = \frac{1}{2} + \Gamma_{IJ}^{(2)} + \Gamma_{IJ}^{(4)} \tag{13}$$

where the parameters $\Gamma_{IK}^{(1)}$, $\Gamma_{IJ}^{(2)}$, $\Gamma_{IK}^{(3)}$ and $\Gamma_{IJ}^{(4)}$ are listed in the Appendix B (cf. 48,43].

2.2. Effective viscoelastic damage model for aligned fiber-reinforced polymeric composites

Viscoelastic materials such as polymers cannot be directly characterized using the conventional elastic analysis employed to obtain the properties of elastic solids [24]. Alternatively, the Boltzmann superposition principle can be conveniently applied to explicitly consider the viscous nature of a polymer [14]. Based on the principle of superposition, the stress response according to the strain–time history can be expressed as [11]

$$\sigma(t) = \sum_{i=1}^{n}\triangle\epsilon_i C(t - \tau_i) \tag{14}$$

where t and τ_i signify the arbitrary time and the time under instantaneous application of $\Delta\epsilon_i$, respectively, and $C(t)$ is the relaxation modulus, which becomes zero for $-\infty \leqslant t \leqslant 0$ [11]. In order to make use of the principle of superposition, let us take the Laplace transform (LT) of Eq. (14) as [14,34,24]

$$\tilde{\sigma}_{ij}(s) = s\widetilde{C}_{ijkl}(s)\tilde{\epsilon}_{kl}(s) \tag{15}$$

where the tilde ($\sim$) signifies the transformed domain (TD) and s is the Laplace constant. By taking LT of Eq. (14), the viscoelastic moduli can be applied into a micromechanical model [14,34,35]. Details of the Laplace-transformed superposition principle among elastic, viscoelastic, and LT of the composite can be found in [14,34,24].

The effective viscoelastic moduli can be derived by replacing the elastic phase with the viscoelastic phase [14,34,35]. The constitutive equation in TD form $[\mathbf{C}^*]^{TD}$ can be written as

$$[\mathbf{C}^*]^{TD} = \left[C_{IK}^{(1)}\right]^{TD}\delta_{ij}\delta_{kl} + \left[C_{IJ}^{(2)}\right]^{TD}(\delta_{ik}\delta_{jl} + \delta_{il}\delta_{jk}) \tag{16}$$

where the second-rank tensor in TD form $\left[C_{IK}^{(1)}\right]^{TD}$ and $\left[C_{IJ}^{(2)}\right]^{TD}$ can be derived by replacing the elastic phase with the LT phase as (cf. 48,43]

$$\left[C_{IK}^{(1)}\right]^{TD} = 2\left\{\mu_0^{TD}\left[\psi_{IK}^{(1)}\right]^{TD} + \lambda_0^{TD}\left[\psi_{KK}^{(2)}\right]^{TD}\right\} + \lambda_0^{TD}\sum_{n=1}^{2}\left[\psi_{nK}^{(1)}\right]^{TD} \tag{17}$$

$$\left[C_{IJ}^{(2)}\right]^{TD} = 2\mu_0^{TD}\left[\psi_{IJ}^{(2)}\right]^{TD} \tag{18}$$

with

$$\begin{aligned}\left[\psi_{IK}^{(1)}\right]^{TD} &= \left[\Gamma_{IK}^{(1)}\right]^{TD} + \left[\Gamma_{IK}^{(3)}\right]^{TD}, \quad \left[\psi_{IJ}^{(2)}\right]^{TD} \\ &= \frac{1}{2} + \left[\Gamma_{IJ}^{(2)}\right]^{TD} + \left[\Gamma_{IJ}^{(4)}\right]^{TD}\end{aligned} \tag{19}$$

where the second-rank tensors $\left[\Gamma_{IK}^{(1)}\right]^{TD}$, $\left[\Gamma_{IJ}^{(2)}\right]^{TD}$, $\left[\Gamma_{IK}^{(3)}\right]^{TD}$ and $\left[\Gamma_{IJ}^{(4)}\right]^{TD}$ are listed in the Appendix C. In addition, λ_0^{TD} and μ_0^{TD} are the LT of the Láme constants and are defined as [34,35]

$$\lambda_0^{TD} = \kappa_0^{TD} - \frac{2\mu_0^{TD}}{3}, \quad \kappa_0^{TD} = \frac{\eta_0\kappa_0 s}{\mu_0 + s\eta_0}, \quad \mu_0^{TD} = \frac{\eta_0\mu_0 s}{\mu_0 + s\eta_0} \tag{20}$$

in which κ_0 and η_0 denote the bulk modulus and the viscosity of matrix, respectively. Moreover, the LT of Poisson's ratio v_0^{TD} of discontinuous fiber-reinforced composites are obtained through the following relation

$$v_0^{TD} = \frac{3\kappa_0^{TD} - 2\mu_0^{TD}}{6\kappa_0^{TD} + 2\mu_0^{TD}} \tag{21}$$

The effective viscoelasticity tensor of the aligned discontinuous fiber-reinforced polymeric composites can be derived as

$$\mathbf{C}^*(t) = C_{IK}^{(1)}(t)\delta_{ij}\delta_{kl} + C_{IJ}^{(2)}(t)(\delta_{ik}\delta_{jl} + \delta_{il}\delta_{jk}) \tag{22}$$

where the parameters $C_{IK}^{(1)}(t)$ and $C_{IJ}^{(2)}(t)$ can be obtained by taking the direct inverse Laplace transform of Eqs. (17) and (18).

2.3. Effective viscoelastic moduli of randomly oriented discontinuous fiber-reinforced composites

In this subsection, we consider polymeric composites in which discontinuous fiber reinforcements are randomly oriented in a 3D space (cf. 43]. In order to obtain the effective viscoelastic moduli with 3D randomly dispersed fibers, the averaging process over 1–3 plane orientations of the governing equation is carried out as defined in the following equation [36,40]:

$$\langle\mathbf{C}\rangle = \frac{\int_{-\pi}^{\pi}\int_{0}^{\pi}\int_{0}^{\pi/2}\overline{C}(\phi,\gamma,\psi)\sin\gamma d\phi\, d\gamma\, d\psi}{\int_{-\pi}^{\pi}\int_{0}^{\pi}\int_{0}^{\pi/2}\sin\gamma d\phi\, d\gamma\, d\psi} \tag{23}$$

where $\langle\rangle$ denotes the 3D orientation average process and $\overline{C}_{ijkl} = c_{ip}c_{jp}c_{kr}c_{ls}C_{pqrs}$, in which c_{ij} are the direction cosine from the local fiber coordinates to the global coordinates (cf. 30,43], and is given by

$$[c_{ij}] = \begin{bmatrix}\cos\theta & \sin\theta & 0\\ -\sin\theta & \cos\theta & 0\\ 0 & 0 & 1\end{bmatrix} \tag{24}$$

After a lengthy algebra in accordance with the aforementioned process, the components of the effective fourth-rank tensor $\langle\mathbf{C}^*(t)\rangle$ read

$$\langle\mathbf{C}^*(t)\rangle = \breve{C}_1(t)\delta_{ij}\delta_{kl} + \breve{C}_2(t)(\delta_{ik}\delta_{jl} + \delta_{il}\delta_{jk}) \tag{25}$$

where

$$\begin{aligned}\breve{C}_1(t) = \frac{1}{15}\Big\{&C_{11}^{(1)}(t) + 4C_{12}^{(1)}(t) + 4C_{21}^{(1)}(t) + 6C_{22}^{(1)}(t) + 2C_{11}^{(2)}(t)\\ &- 4C_{12}^{(2)}(t) + 2C_{22}^{(2)}(t)\Big\}\end{aligned} \tag{26}$$

$$\begin{aligned}\breve{C}_2(t) = \frac{1}{15}\Big\{&C_{11}^{(1)}(t) - C_{12}^{(1)}(t) - C_{21}^{(1)}(t) + C_{22}^{(1)}(t) + 2C_{11}^{(2)}(t)\\ &+ 6C_{12}^{(2)}(t) + 7C_{22}^{(2)}(t)\Big\}\end{aligned} \tag{27}$$

Details of the averaging process over 3D orientations of the governing equation can be found in [36,30,31,40,43].

3. Strain rate sensitivity of polymeric composites

The strain rate affects the overall behavior of polymeric materials and can be therefore an important consideration for an accurate prediction [41]. However, owing to the complexity of determining the strain rate sensitivity, only a few micromechanical studies have investigated the correlation between the strain rate and the behavior of polymeric composites [7]. The present study adopts a modified Maxwell model [51] for the modeling of the strain rate sensitivity of a polymer matrix.

The Maxwell model is widely used for viscoelastic modeling since it accurately predicts how the stress in most polymers decays exponentially with time [38]. The spring stands for the elastic modulus E_0 of the polymer matrix; and the damper, on the other hand, signifies the viscosity η_0 of the matrix. Thus, the widely known single Maxwell model [11] can be expressed as follows:

$$\dot{\epsilon}(t) = \frac{\dot{\sigma}(t)}{E_0} + \frac{\sigma(t)}{\eta_0} \tag{28}$$

Following [51] considering the first-order linear differential equation theory, Eq. (28) can be rewritten as

$$\sigma(t) = E_0\int_0^t \exp\left(\frac{-E_0(t-\tau)}{\eta_0}\right)\dot{\epsilon}(\tau)\mathrm{d}\tau \tag{29}$$

When consideration is given to a special but useful condition that enables the strain rate to remain constant throughout the test period, Eq. (29) can be rephrased as [51]:

$$\sigma(t) = \dot{\epsilon}\eta_0\left\{1 - \exp\left(\frac{-tE_0}{\eta_0}\right)\right\} \tag{30}$$

In addition, the constitutive equation for a constant strain rate, which can be obtained by substituting $t = \epsilon(t)/\dot{\epsilon}$, can be used to estimate the viscosity of a polymer matrix.

Fig. 1 shows the algorithm for the inverse analysis. In the present study, a Newton–Raphson method the using the modified

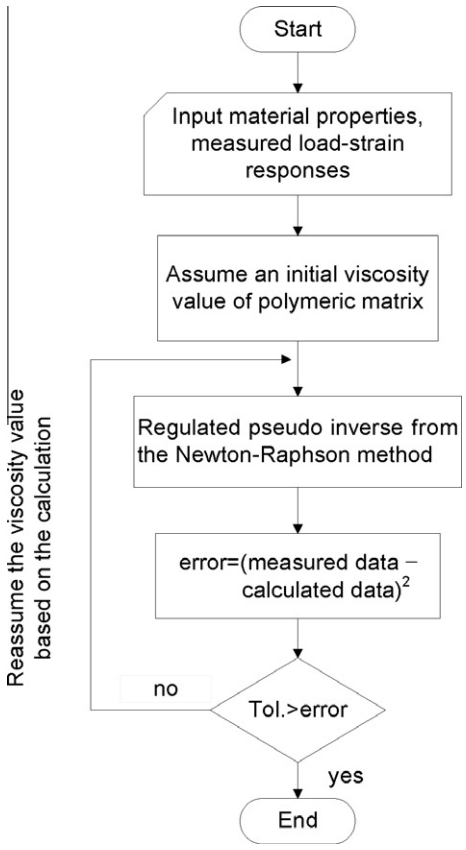

Fig. 1. The algorithm for the inverse analysis for obtaining the viscosity property of a polymeric matrix.

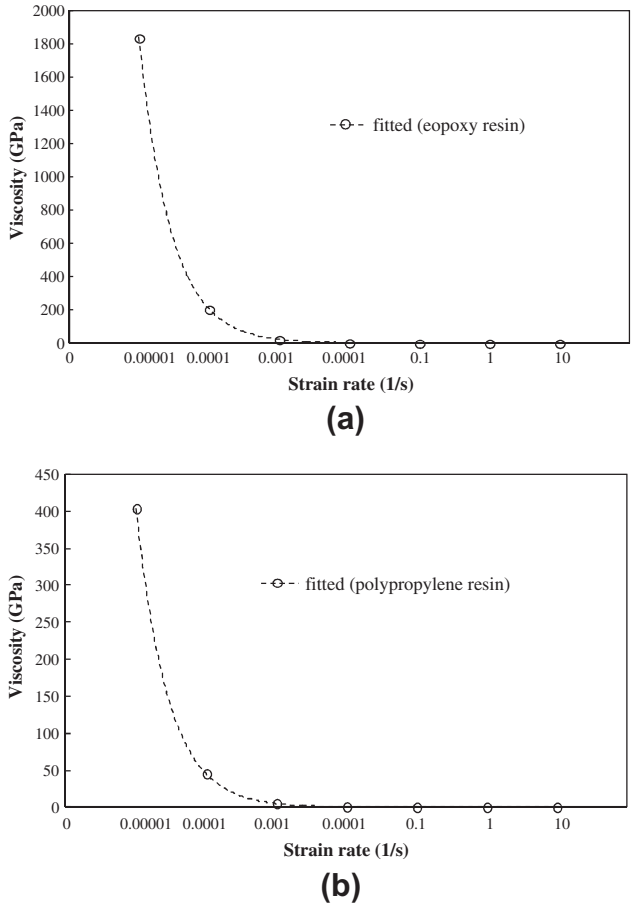

Fig. 2. Relationship between viscosity (η) and strain rate ($\dot{\epsilon}$) of epoxy resin (a) and polypropylene resin (b).

Maxwell model [51] is used for calculating the viscosity property of the matrix. The Newton–Raphson method is repeatedly performed, and the viscosity of the matrix is estimated against the experimental data [13,7] until the error becomes less than a given tolerance. Accordingly, the viscosity of an epoxy matrix can be calculated as [13]

$$\eta_0 = 31.6\exp\{-2.194\cdot\log(\dot{\epsilon})\} \tag{31}$$

Similarly, the viscosity of a polypropylene matrix [7] can also be obtained as

$$\eta_0 = 7.2\exp\{-2.187\cdot\log(\dot{\epsilon})\} \tag{32}$$

The relationship between the obtained viscosity function η_0 and the strain rate $\dot{\epsilon}$ of the epoxy matrix and the polypropylene matrix is shown in Fig. 2a and b, respectively. It is observed from the figures that the curve decreases exponentially with the increase of the constant strain rate [42].

The above-mentioned approach is verified by incorporating the calculated viscosity functions into the micromechanical model (Eq. (20)). [13] conducted a stress–strain test on the epoxy matrix under different constant strain rates ($\dot{\epsilon} = 1.3$ and 0.00006/s). Their results are compared with the present predictions, which are subjected to the same constant strain rate as used in the experiment as shown in Fig. 3a. Fig. 3b shows comparisons between the results of the proposed model and the experimental results on the polypropylene matrix with various constant strain rates ($\dot{\epsilon} = 115$, 11.5, 1.15, 0.115, 0.0115, and 0.00115/s). It is noted that the volume fraction of discontinuous fibers is assumed to be zero ($\phi_1 = 0\%$) in the simulations since the experiment was carried out on a pure polymer matrix. Fig. 3a shows that the prediction results of the proposed model, which considers the strain rate effect, are in agreement with the experimental data. The predictions of early stage of the stress–strain responses do not match well with the experimental data, whereas relatively good agreements between the present predictions and the experimental data are observed beyond $\epsilon = 0.02$ from Fig. 3b.

4. Numerical simulations

In this section, a series of numerical simulations based on the proposed model are carried out to investigate the influence of the damage parameter S_0, the strain rate $\dot{\epsilon}$, the aspect ratio of fibers α, and fiber orientation characteristics on the behavior of composites. For the present numerical simulations, we adopt the material properties of discontinuous glass fiber-reinforced polypropylene matrix composites in accordance with [10] as: $E_0 = 1.30$ GPa, $v_0 = 0.36$, and $\eta_0 = 7.2\exp\{-2.1868\cdot\log(\dot{\epsilon})\}$; E_1=78.51 GPa, v_1=0.16, and ϕ_1=25%. The spherical shape ($\alpha = 1$) and two sets of the aspect ratio ($\alpha = 0.2$, 5) for both orientation cases (unidirectionally aligned; randomly oriented) are considered in the simulations. The damage parameters and strain rate are fixed as $S_0 = 600$ MPa, $M = 2$; $\dot{\epsilon} = 0.0001/\text{s}$. The predicted stress–strain responses of a polymeric composite are exhibited in Fig. 4. It is shown from the figure that the stress–strain response becomes stiffer as α continues to increase for both orientation cases. It is also observed that the effect of the aspect ratio is more pronounced in the case of the unidirectionally aligned fiber-reinforced composites.

In order to evaluate the influence of the strain rate $\dot{\epsilon}$, four different strain rates ($\dot{\epsilon} = 0.001$, 0.0001, 0.00001, and 0.000001/s) are considered here. The same damage parameters as previously used are utilized, and the aspect ratio is assumed as $\alpha = 5$. Fig. 5 shows

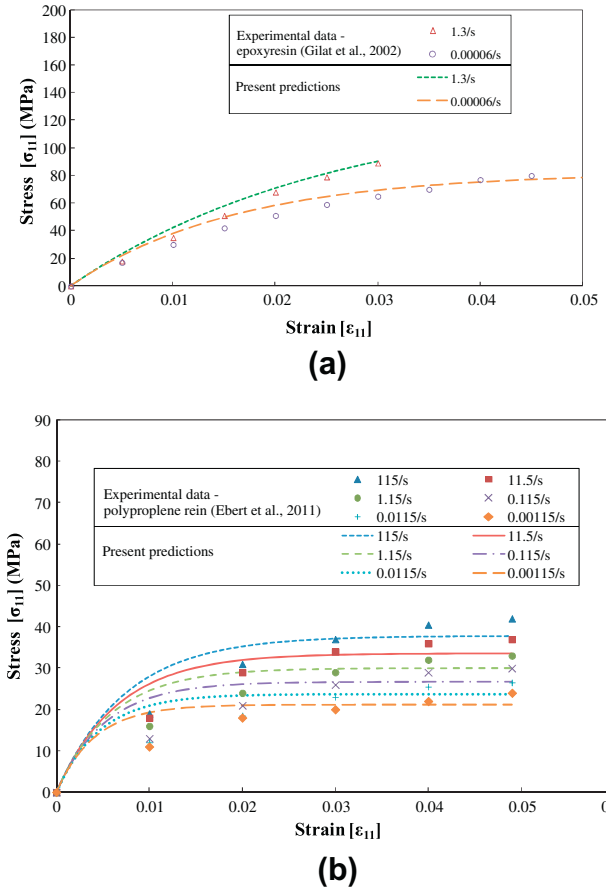

Fig. 3. Comparisons of the stress–strain responses of the epoxy resin [13] (a) and the polypropylene matrix [7] (b) with respect to various strain rates.

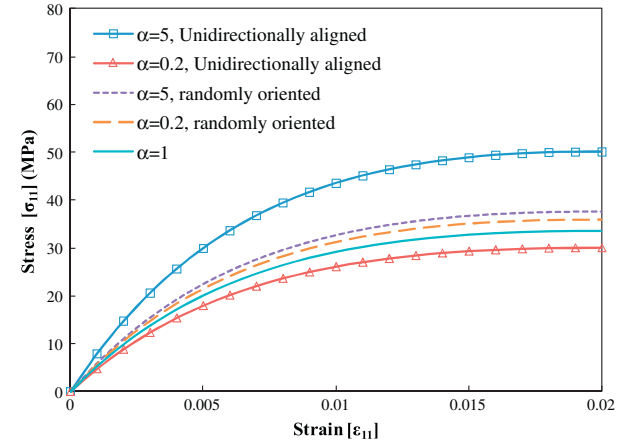

Fig. 4. The predicted stress–strain curves of aligned and 3D randomly oriented fiberreinforced polymeric composites considering various aspect ratios.

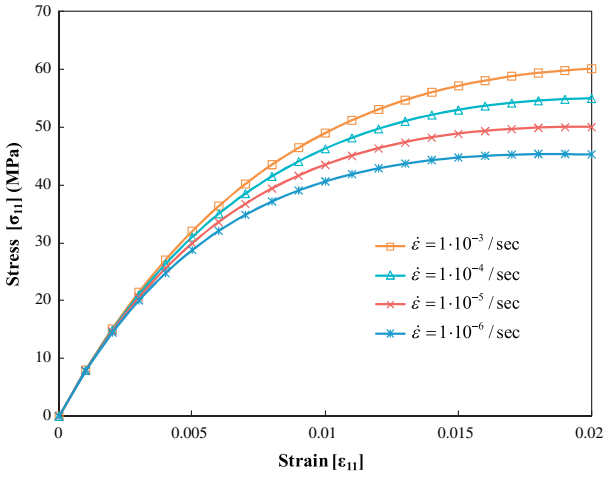

Fig. 5. Influence of the strain rate on the overall viscoelastic stress–strain behavior of aligned discontinuous fiber-reinforced polymeric composites.

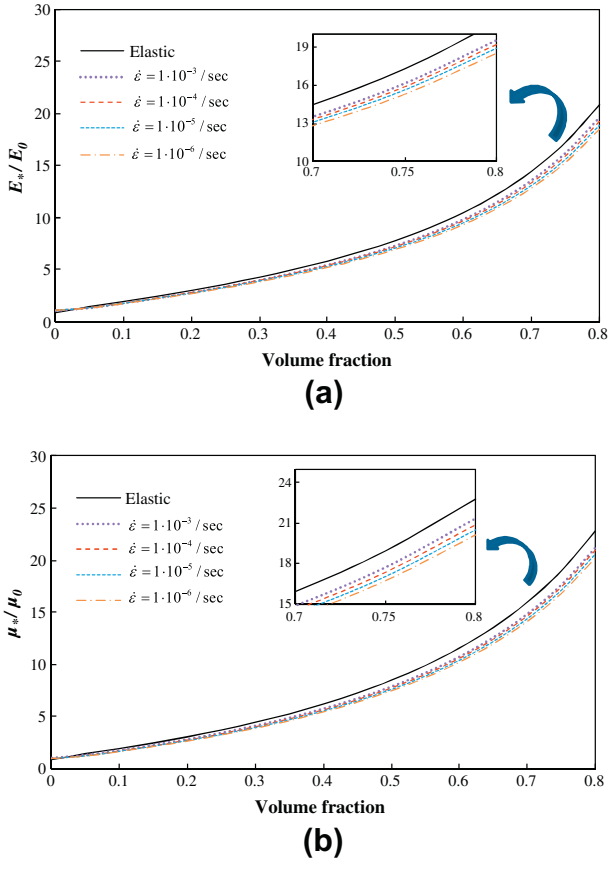

Fig. 6. The predicted normalized Young's (a) and shear moduli (b) of discontinuous fiberreinforced polymeric composites with various strain rates versus fiber volume fraction.

the predicted stress–strain responses with various strain rates. In addition, the predicted normalized Young's and shear moduli of the composites under different strain rates are presented in Fig. 6a and b, respectively. Figs. 5 and 6 show that the strain rate affects the overall viscoelastic behavior of the composites, and the viscous property becomes more pronounced as the strain rate decreases.

To further examine the effect of the damage parameter S_0, which is related to the interfacial strength between discontinuous fibers and the matrix, on the behavior of the composites, a parametric analysis with various S_0 values is conducted. The predicted stress–strain responses with various S_0 values are plotted in Fig. 7a. The evolution of damaged discontinuous fibers corresponding to Fig. 7a is depicted in Fig. 7b. The strain–stress curves increases slightly as the damage parameter S_0 increases. It is also found that discontinuous fibers evolve more rapidly to damaged fibers as the damage parameter S_0 decreases. Biaxial and hydrostatic tensile tests on the composites are also performed to

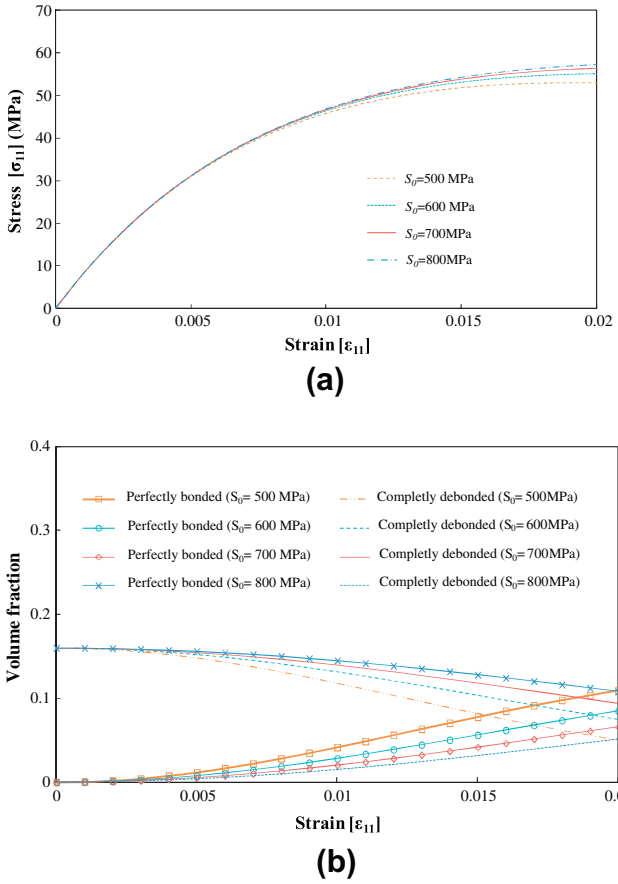

Fig. 7. (a) The predicted stress–strain responses under uniaxial tension with various S_0 values; (b) the damage evolution versus strain with various S_0 values the corresponding to (a).

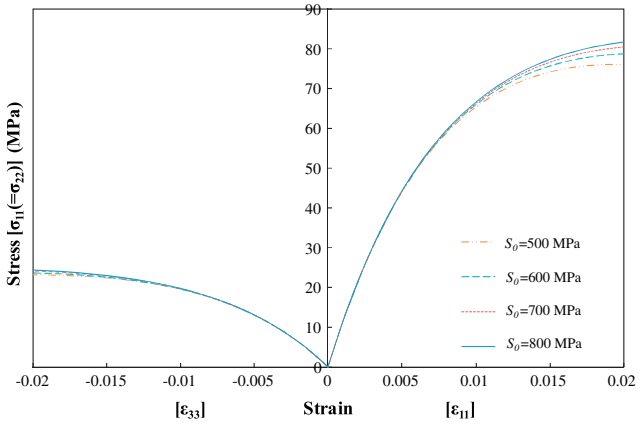

Fig. 8. The predicted stress–strain responses of discontinuous fiber-reinforced polymeric composites under biaxial loading with various S_0 values.

examine the viscoelastic stress–strain response under different loading conditions. The predicted biaxial and hydrostatic stress–strain responses with various S_0 values are exhibited in Figs. 8 and 9, respectively. Similar to the uniaxial loading condition, higher S_0 leads to a stiffer stress–strain response.

The influence of the aspect ratio of fibers α on the predicted stress–strain responses of composites containing aligned and 3D randomly oriented fibers are shown in Fig. 10a and b. The same material properties, damage parameters, and strain rate as used in the previous simulations are utilized. Four different aspect ratios

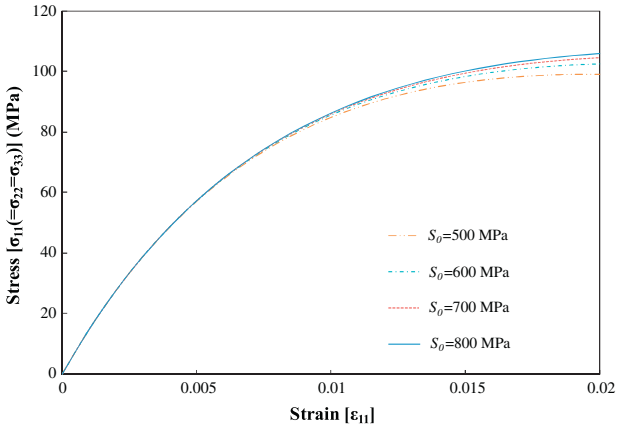

Fig. 9. The predicted stress–strain responses of discontinuous fiber-reinforced polymeric composites under hydrostatic loading with various S_0 values.

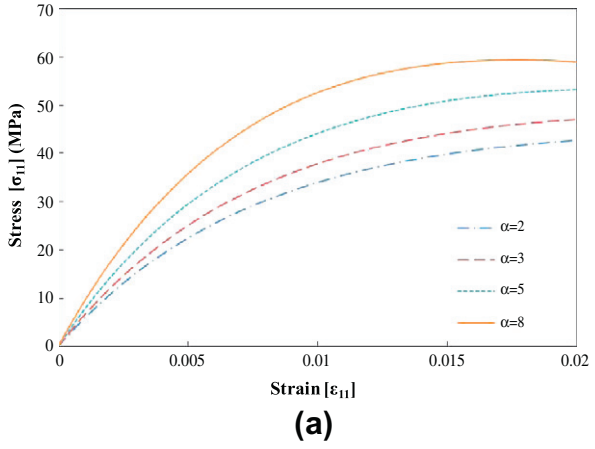

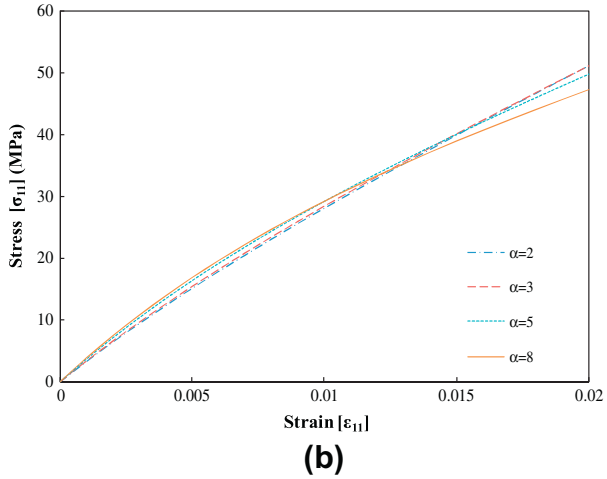

Fig. 10. The predicted stress–strain curves of unidirectionally aligned (a) and 3D randomly oriented (b) discontinuous fiber-reinforced polymeric composites with various aspect ratios.

(α = 2, 3, 5, 8) are considered. It is clear from the figures that the aspect ratio is quite influential in the case of unidirectionally aligned fiber-reinforced polymeric composites compared with 3D randomly oriented fiber-reinforced composites. Conversely, lower stress–strain responses are obtained from 3D randomly oriented fiber-reinforced composites as α increases.

The predicted stress–strain responses of aligned and 3D randomly oriented fiber-reinforced polymeric composites with

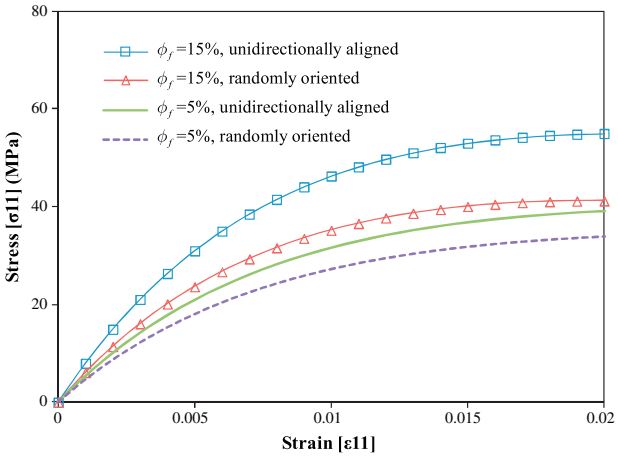

Fig. 11. The predicted stress–strain curves of unidirectionally aligned and 3D randomly oriented discontinuous fiber-reinforced polymeric composites with various fiber volume fractions.

different fiber volume fractions are presented in Fig. 11. The maximum stress–strain response is exhibited at ϕ = 15% under uniaxial loading condition.

5. Experimental comparisons

Predictions based on the proposed model are compared with experimental data to further assess the predictive capacity of the present framework. Two sets of experimental data for aligned and 3D randomly oriented discontinuous fiber-reinforced polymeric composites [10,39] are chosen for comparisons.

First, predictions on aligned glass fiber-reinforced polypropylene matrix composites with two different fiber volume fractions (ϕ = 8%, 16%) are made with the same material properties as reported in [10] as: E_0 = 1.30 GPa, v_0 = 0.36, and $\eta_0 = 7.2\exp\{-2.1868\cdot\log(\dot{\epsilon})\}$; and E_1 = 78.51 GPa, v_1 = 0.25, and α = 50. Since the damage parameters S_0 and M were not reported in [10], they are estimated following an experimentally derived stress–strain curve reported in [10] as: S_0 = 350 MPa and M = 2. The strain rate is assumed to be $\dot{\epsilon} = 0.00001/\mathrm{s}$. The model parameters are fitted at ϕ_1=16%; it should be noted that the same estimated values for the parameters are applied to the ϕ_1 = 8% case. Fig. 12 shows the comparison of the stress–strain curves of glass fiber-reinforced

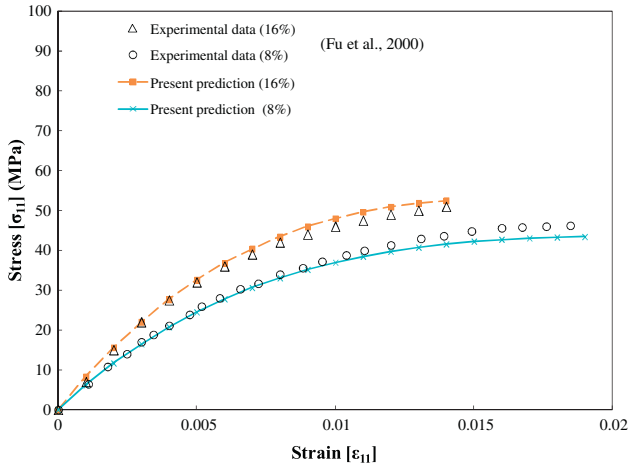

Fig. 12. Comparisons of the stress–strain curves of glass fiber-reinforced polypropylene matrix composites with various fiber volume fractions (ϕ = 8%, 16%) between the proposed micromechanics-based viscoelastic model and experimental data [10].

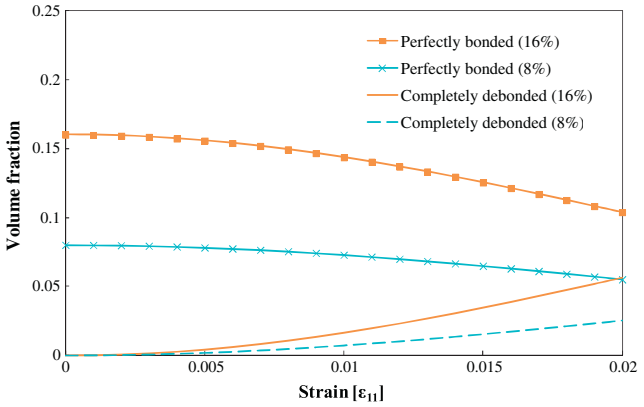

Fig. 13. The predicted damage evolution of discontinuous fiber-reinforced polymeric composites (8%, 16%) corresponding to Fig. 12.

polypropylene matrix composites with various fiber volume fractions (ϕ = 8%, 16%) between the proposed micromechanics-based viscoelastic model and experimental data [10]. The predicted uniaxial stress–strain responses are shown to be a good agreement with the experimental data. The predicted evolution of damaged fibers corresponding to Fig. 12 is shown in Fig. 13.

The present predictions on 3D randomly oriented discontinuous fiber-reinforced polymeric composites are compared with the experimental data [39]. Similarly, the same material properties

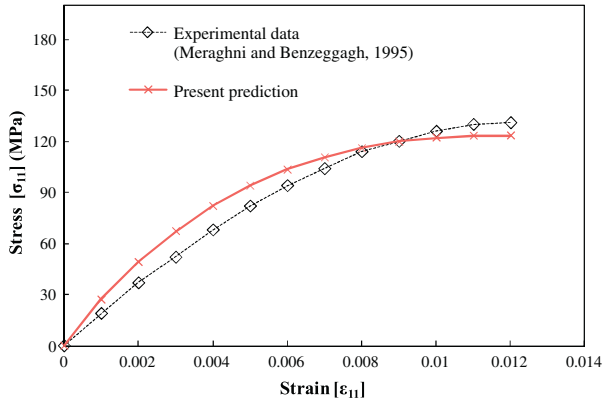

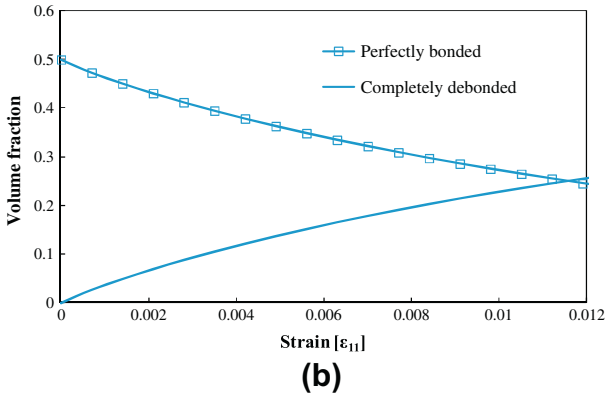

Fig. 14. (a) The comparison of stress–strain curves of discontinuous glass fiber, epoxy matrix composites between the prediction and experimental data (Meraghni and Benzeggagh, 1995); (b) the predicted damage evolution as a function of the strain of the discontinuous fiber-reinforced polymeric composites corresponding to (a).

as reported in [39] are utilized as: E_0=3.0 GPa, ν_0=0.35, and $\eta_0 = 31.557\exp\{-2.194\cdot\log(\dot{\epsilon})\}$; and E_1 = 72 GPa, ν_1 = 0.17, α = 19.5, and ϕ_1 = 50%. The damage parameters and strain rate are fitted as: S_0 = 1.5 GPa, M = 0.9, and $\dot{\epsilon} = 0.00003/s$. Fig. 14a show the overall stress–strain response of the 3D randomly oriented fiber-reinforced polymeric composites under uniaxial tensile stress. In addition, Fig. 14b shows the predicted progression of the volume fractions of damaged fibers corresponding to Fig. 14a. Another good agreement between the present predictions and the experimental data on 3D randomly oriented fiber-reinforced polymeric composites is observed from the Fig. 14a.

The aforementioned comparative results may highlight the predictive capacity of the proposed micromechanical framework for predicting the viscoelasticity of discontinuous fiber-reinforced polymeric composites.

6. Concluding remarks

A micromechanical viscoelastic damage model has been proposed for aligned and 3D randomly oriented discontinuous fiber-reinforced polymeric composites. The model, which predicts the effective viscoelastic stress–strain behavior of the composites, is based on a combination of the Laplace-transformed superposition principle and the ensemble-averaged micromechanics [34,18,19]. Weibull's probabilistic function [52,20] is applied to the proposed model to characterize the evolution of damaged fibers. An inverse analysis is carried out to take into account the strain rate sensitivity of the polymer matrix. A series of numerical simulations are conducted to examine the influence of the damage parameters and strain rates; and different loading conditions are applied on the proposed model for the purpose of predicting the stress–strain responses. In addition, experimental comparisons are conducted to present and assess the predictive capability of the proposed model. The findings from a series of numerical simulations and comparisons can be summarized as follows:

(1) The aspect ratio α has a significantly effect on the aligned fiber-reinforced composites but has a marginal effect on 3D randomly oriented fiber-reinforced composites.
(2) The Weibull's probability damage parameters are related to the damage evolution of the reinforcements in the composites, and higher S_0 values lead to higher levels of stress–strain behavior.
(3) The effects of the aspect ratio on the viscoelastic composites are quite influential. A larger aspect ratio results in a higher stress–strain response in aligned fiber reinforcements, while 3D randomly oriented fiber-reinforced composites produce inverse results: a higher stress–strain response is obtained with a smaller aspect ratio.
(4) The strain rate affects the overall behavior of viscoelastic composites. A higher strain rate leads to a weak viscous property and the behavior consequently becomes more elastic.

This study demonstrates the predictive capability of the proposed micromechanics-based viscoelastic damage model. The model is particularly suitable for predicting the behavior of aligned and 3D randomly orientated discontinuous fiber-reinforced polymeric composites. However, additional experimental and numerical tests are still needed to assess the parameters used in the proposed model.

Acknowledgments

This research was supported by grants from the Construction Technology Innovation Program (11CCTI-B050520-04-000000) and the U-City Master and Doctor Course Grant Program (07High Tech A01) funded by the Ministry of Land, Transportation and Maritime Affairs of the Korean government.

Appendix A. The damage parameters $L_{IK}^{(1)}$, $L_{IJ}^{(2)}$, $L_{IK}^{(3)}$, and $L_{IJ}^{(4)}$ in Eq. (10)

$$L_{IK}^{(2r-1)} = \frac{\phi_r}{4(1-\nu_0)}\left\{2S_{IK}^{(2r-1)}\zeta_{KK}^{(2r)} + 2S_{II}^{(2r)}\zeta_{IK}^{(2r-1)} + \sum_{n=1}^{3} S_{In}^{(2r-1)}\zeta_{nK}^{(2r-1)}\right\}, \quad (r=1,2) \tag{33}$$

$$L_{IJ}^{(2r)} = \frac{\phi_r}{2(1-\nu_0)} S_{IJ}^{(2r)}\zeta_{IJ}^{(2r)}, \quad (r=1,2) \tag{34}$$

in which

$$\zeta_{IK}^{(1)} = -\frac{2(1-\nu_0)\Upsilon_{IK}^{(1)}}{\acute{\mu}+S_{II}^{(2)}}, \quad \zeta_{IJ}^{(2)} = \frac{1-\nu_0}{\acute{\mu}+S_{IJ}^{(2)}} \tag{35}$$

$$\zeta_{IK}^{(3)} = -\Upsilon_{IK}^{(2)} + \frac{S_{II}^{(2)}\Upsilon_{IK}^{(2)}}{-2(1-\nu_0)+S_{II}^{(2)}}, \quad \zeta_{IJ}^{(4)} = \frac{S_{IJ}^{(2)}(1-\nu_0)}{1-2S_{IJ}^{(2)}(1-\nu_0)} \tag{36}$$

with

$$\Upsilon_{I1}^{(1)} = \frac{\left(\acute{\lambda}+\acute{\mu}+S_{22}^{(1)}+S_{22}^{(2)}\right)\left(\acute{\lambda}+S_{I1}^{(1)}\right) - \left(\acute{\lambda}+S_{21}^{(1)}\right)\left(\acute{\lambda}+S_{I2}^{(1)}\right)}{\left(\acute{\lambda}+\acute{\mu}+S_{22}^{(1)}+S_{22}^{(2)}\right)\left(\acute{\lambda}+2\acute{\mu}+S_{11}^{(1)}+S_{12}^{(2)}\right) - \left(\acute{\lambda}+S_{12}^{(1)}\right)\left(\acute{\lambda}+S_{21}^{(1)}\right)} \tag{37}$$

$$\Upsilon_{I2}^{(1)} = \Upsilon_{I3}^{(1)} = \frac{\left(\acute{\lambda}+2\acute{\mu}+S_{11}^{(1)}+2S_{11}^{(2)}\right)\left(\acute{\lambda}+S_{I2}^{(1)}\right) - \left(\acute{\lambda}+S_{12}^{(1)}\right)\left(\acute{\lambda}+S_{I1}^{(1)}\right)}{2\left(\acute{\lambda}+\acute{\mu}+S_{22}^{(1)}+S_{22}^{(2)}\right)\left(\acute{\lambda}+2\acute{\mu}+S_{11}^{(1)}+2S_{11}^{(2)}\right) - 2\left(\acute{\lambda}+S_{12}^{(1)}\right)\left(\acute{\lambda}+S_{21}^{(1)}\right)} \tag{38}$$

$$\Upsilon_{I1}^{(2)} = \frac{\left\{S_{22}^{(1)}+S_{22}^{(2)}-2(1-\nu_0)\right\}S_{I1}^{(1)} - S_{21}^{(1)}S_{I2}^{(1)}}{\left\{S_{22}^{(1)}+S_{22}^{(2)}-2(1-\nu_0)\right\}\left\{S_{11}^{(1)}+2S_{11}^{(2)}-4(1-\nu_0)\right\} - S_{12}^{(1)}S_{21}^{(1)}} \tag{39}$$

$$\Upsilon_{I2}^{(2)} = \Upsilon_{I3}^{(2)} = \frac{\left\{S_{11}^{(1)}+2S_{11}^{(2)}-4(1-\nu_0)\right\}S_{I2}^{(1)} - S_{12}^{(1)}S_{I1}^{(1)}}{2\left\{S_{22}^{(1)}+S_{22}^{(2)}-2(1-\nu_0)\right\}\left\{S_{11}^{(1)}+2S_{11}^{(2)}-4(1-\nu_0)\right\} - 2S_{12}^{(1)}S_{21}^{(1)}} \tag{40}$$

Appendix B. The elastic parameters $\Gamma_{IK}^{(1)}$, $\Gamma_{IJ}^{(2)}$, $\Gamma_{IK}^{(3)}$ and $\Gamma_{IJ}^{(4)}$ in Eq. (13)

$$\Gamma_{IK}^{(2r-1)} = \phi_r\left\{2\left(\zeta_{IK}^{(2r-1)}\varpi_{KK}^{(2r)} + \zeta_{II}^{(2r)}\varpi_{IK}^{(2r-1)}\right) + \sum_{n=1}^{3}\zeta_{In}^{(2r-1)}\varpi_{nK}^{(2r-1)}\right\}, \quad (r=1,2) \tag{41}$$

$$\Gamma_{IJ}^{(2r)} = 2\phi_r\zeta_{IJ}^{(2r)}\varpi_{IJ}^{(2r)}, \quad (r=1,2) \tag{42}$$

in which

$$\varpi_{IK}^{(2r-1)} = \frac{\Lambda_{IK}^{(r)}}{1-2L_{II}^{(2r)}}, \quad \varpi_{IJ}^{(2r)} = \frac{1}{2\left(1-2L_{IJ}^{(2r)}\right)} \tag{43}$$

with

$$\Lambda_{I1}^{(r)} = \frac{\left\{\frac{1}{2} - L_{22}^{(2r-1)} - L_{22}^{(2r)}\right\}L_{I1}^{(2r-1)} + L_{21}^{(2r-1)}L_{I2}^{(2r-1)}}{\left\{\frac{1}{2} - L_{22}^{(2r-1)} - L_{22}^{(2r)}\right\}\left\{1 - L_{11}^{(2r-1)} - 2L_{11}^{(2r)}\right\} - L_{12}^{(2r-1)}L_{21}^{(2r-1)}} \tag{44}$$

$$\Lambda_{I2}^{(r)} = \Lambda_{I3}^{(r)} = \frac{\left\{1 - L_{11}^{(2r-1)} - 2L_{11}^{(2r)}\right\}L_{I2}^{(2r-1)} + L_{12}^{(2r-1)}L_{I1}^{(2r-1)}}{2\left\{\frac{1}{2} - L_{22}^{(2r-1)} - L_{22}^{(2r)}\right\}\left\{1 - L_{11}^{(2r-1)} - 2L_{11}^{(2r)}\right\} - L_{12}^{(2r-1)}L_{21}^{(2r-1)}} \tag{45}$$

Appendix C. The parameters of LT $\left[\Gamma_{IK}^{(1)}\right]^{TD}$, $\left[\Gamma_{IJ}^{(2)}\right]^{TD}$, $\left[\Gamma_{IK}^{(3)}\right]^{TD}$ and $\left[\Gamma_{IJ}^{(4)}\right]^{TD}$ in Eq. (19)

These parameters can be obtained by replacing elasitc phase by viscoelasitc phase of matrix as

$$\left[\Gamma_{IK}^{(2r-1)}\right]^{TD} = \phi_r\left\{2\left(\left[\zeta_{IK}^{(2r-1)}\right]^{TD}\left[\varpi_{KK}^{(2r)}\right]^{TD} + \left[\zeta_{II}^{(2r)}\right]^{TD}\left[\varpi_{IK}^{(2r-1)}\right]^{TD}\right) + \sum_{n=1}^{3}\left[\zeta_{In}^{(2r-1)}\right]^{TD}\left[\varpi_{nK}^{(2r-1)}\right]^{TD}\right\} \tag{46}$$

$$\left[\Gamma_{IJ}^{(2r)}\right]^{TD} = 2\phi_r\left[\zeta_{IJ}^{(2r)}\right]^{TD}\left[\varpi_{IJ}^{(2r)}\right]^{TD} \tag{47}$$

in which

$$\left[\varpi_{IK}^{(2r-1)}\right]^{TD} = \frac{\left[\Lambda_{IK}^{(r)}\right]^{TD}}{1 - 2\left[L_{II}^{(2r)}\right]^{TD}}, \quad \left[\varpi_{IJ}^{(2r)}\right]^{TD} = \frac{1}{2\left(1 - 2\left[L_{IJ}^{(2r)}\right]^{TD}\right)} \tag{48}$$

with

$$\left[\Lambda_{I1}^{(r)}\right]^{TD} = \frac{\left\{\frac{1}{2} - \left[L_{22}^{(2r-1)}\right]^{TD} - \left[L_{22}^{(2r)}\right]^{TD}\right\}\left[L_{I1}^{(2r-1)}\right]^{TD} + \left[L_{21}^{(2r-1)}\right]^{TD}\left[L_{I2}^{(2r-1)}\right]^{TD}}{\left\{\frac{1}{2} - \left[L_{22}^{(2r-1)}\right]^{TD} - \left[L_{22}^{(2r)}\right]^{TD}\right\}\left\{1 - \left[L_{11}^{(2r-1)}\right]^{TD} - 2\left[L_{11}^{(2r)}\right]^{TD}\right\} - \left[L_{12}^{(2r-1)}\right]^{TD}\left[L_{21}^{(2r-1)}\right]^{TD}} \tag{49}$$

$$\left[\Lambda_{I2}^{(r)}\right]^{TD} = \left[\Lambda_{I3}^{(r)}\right]^{TD} = \frac{\left\{1 - \left[L_{11}^{(2r-1)}\right]^{TD} - 2\left[L_{11}^{(2r)}\right]^{TD}\right\}\left[L_{I2}^{(2r-1)}\right]^{TD} + \left[L_{12}^{(2r-1)}\right]^{TD}\left[L_{I1}^{(2r-1)}\right]^{TD}}{2\left\{\frac{1}{2} - \left[L_{22}^{(2r-1)}\right]^{TD} - \left[L_{22}^{(2r)}\right]^{TD}\right\}\left\{1 - \left[L_{11}^{(2r-1)}\right]^{TD} - 2\left[L_{11}^{(2r)}\right]^{TD}\right\} - \left[L_{12}^{(2r-1)}\right]^{TD}\left[L_{21}^{(2r-1)}\right]^{TD}} \tag{50}$$

with

$$\left[L_{IK}^{(2r-1)}\right]^{TD} = \frac{\phi_r}{4(1-v_0^{TD})}\left\{2S_{IK}^{(2r-1)}\left[\zeta_{KK}^{(2r)}\right]^{TD} + 2S_{II}^{(2r)}\left[\zeta_{IK}^{(2r-1)}\right]^{TD} + \sum_{n=1}^{3}S_{In}^{(2r-1)}\left[\zeta_{nK}^{(2r-1)}\right]^{TD}\right\} \tag{51}$$

$$\left[L_{IJ}^{(2r)}\right]^{TD} = \frac{\phi_r}{2(1-v_0^{TD})}S_{IJ}^{(2r)}\left[\zeta_{IJ}^{(2r)}\right]^{TD} \tag{52}$$

in which

$$\left[\zeta_{IK}^{(1)}\right]^{TD} = -\frac{2(1-v_0^{TD})\left[\Upsilon_{IK}^{(1)}\right]^{TD}}{\acute{\mu}^{TD} + S_{II}^{(2)}}, \quad \left[\zeta_{IJ}^{(2)}\right]^{TD} = \frac{1-v_0^{TD}}{\acute{\mu}^{TD} + S_{IJ}^{(2)}} \tag{53}$$

with

$$\left[\Upsilon_{I1}^{(1)}\right]^{TD} = \frac{\left(\acute{\lambda}^{TD} + \acute{\mu}^{TD} + S_{22}^{(1)} + S_{22}^{(2)}\right)\left(\acute{\lambda}^{TD} + S_{I1}^{(1)}\right) - \left(\acute{\lambda}^{TD} + S_{21}^{(1)}\right)\left(\acute{\lambda}^{TD} + S_{I2}^{(1)}\right)}{\left(\acute{\lambda}^{TD} + \acute{\mu}^{TD} + S_{22}^{(1)} + S_{22}^{(2)}\right)\left(\acute{\lambda}^{TD} + 2\acute{\mu}^{TD} + S_{11}^{(1)} + S_{12}^{(2)}\right) - \left(\acute{\lambda}^{TD} + S_{12}^{(1)}\right)\left(\acute{\lambda}^{TD} + S_{21}^{(1)}\right)} \tag{54}$$

$$\left[\Upsilon_{I2}^{(1)}\right]^{TD} = \left[\Upsilon_{I3}^{(1)}\right]^{TD} = \frac{\left(\acute{\lambda}^{TD} + 2\acute{\mu}^{TD} + S_{11}^{(1)} + 2S_{11}^{(2)}\right)\left(\acute{\lambda}^{TD} + S_{I2}^{(1)}\right) - \left(\acute{\lambda}^{TD} + S_{12}^{(1)}\right)\left(\acute{\lambda}^{TD} + S_{I1}^{(1)}\right)}{2\left(\acute{\lambda}^{TD} + \acute{\mu}^{TD} + S_{22}^{(1)} + S_{22}^{(2)}\right)\left(\acute{\lambda}^{TD} + 2\acute{\mu}^{TD} + S_{11}^{(1)} + 2S_{11}^{(2)}\right) - 2\left(\acute{\lambda}^{TD} + S_{12}^{(1)}\right)\left(\acute{\lambda}^{TD} + S_{21}^{(1)}\right)} \tag{55}$$

with

$$\acute{\lambda}^{TD} = \frac{4(1-v_0^{TD})(\mu_1\lambda_0^{TD} - \mu_0^{TD}\lambda_1)}{(\mu_1 - \mu_0^{TD})\{3(\lambda_1 - \lambda_0^{TD}) + 2(\mu_1 - \mu_0^{TD}))\}} \tag{56}$$

$$\acute{\mu}^{TD} = \frac{2\mu_0^{TD}(1-v_0^{TD})}{\mu_1 - \mu_0^{TD}} \tag{57}$$

where the LT of Láme constants λ_0^{TD} and μ_0^{TD} are defined in Eq. (20), and Poisson's ratio in LT v_0^{TD} is defined in Eq. (21), respectively.

References

[1] Casula G, Carcione JM. Generalized mechanical model analogies of linear viscoelastic behaviour. Bollettino di Geofisica Teorica ed Applicata 1992;34:235–56.
[2] Chang S, Bert CW. Analysis of damping for filamentary composite materials. In: Proceedings of the sixth St. Louis symposium. American Society of Metals; 1973.
[3] Christensen RM, Lo KH. Solutions for effective shear properties in three phase sphere and cylinder models. J Mech Phys Solids 1979;27:315–30.
[4] Dai LH, Ling Z, Bai YL. Size-dependent inelastic behavior of particle-reinforced metal-matrix composites. Compos Sci Technol 2001;61:1057–63.
[5] Das JN, Nair NG, Subramaniam N. In-plane and transverse damping characteristics of short-fiber-reinforced bromobutyl rubber composites. Rubber Compos: Process Appl 1993;22:249–55.
[6] Dubenets VG, Yakovenko OA. Determination of effective damping characteristics of fiber-reinforced viscoelastic composites. Strength Mater 2009;41:436–43.
[7] Ebert C, Hufenbach W, Langkamp A, Gude M. Modelling of strain rate dependent deformation behaviour of polypropylene. Polym Test 2011;30:183–7.
[8] Ellyin F, Xia Z, Chen Y. Viscoelastic micromechanical modeling of free edge and time effects in glass fiber/epoxy cross-ply laminates. Compos Part A: Appl Sci Manufact 2002;33:399–409.
[9] Eshelby JD. The determination of the field of an ellipsoidal inclusion and related problems. Proc Roy Soc Lond, Ser A: Math Phys Sci 1957;241:376–96.
[10] Fu SY, Lauke B, Mader E, Yue CY, Hu X. Tensile properties of short-glass-fiber- and short-carbon-fiber-reinforced polypropylene composites. Compos Part A: Appl Sci Manufact 2000;31:1117–25.
[11] Gibson RF. Principles of composites material mechanics. McGraw-Hill; 1994.
[12] Gibson RF, Chaturvedi SK, Sun CT. Complex moduli of aligned discontinuous fibre-reinforced polymer composites. J Mater Sci 1982;17:3499–509.
[13] Gilat A, Goldberg RK, Roberts GD. Experimental study of strain-rate-dependent behavior of carbon/epoxy composite. Compos Sci Technol 2002;62:1469–76.
[14] Hashin Z. Complex moduli of viscoelastic composites I: general theory and application to particulate composites. Int J Solids Struct 1970;6:539–52.
[15] Hashin Z. Thermoelastic properties of fiber composites with imperfect interface. Mech Mater 1990;8:333–48.
[16] Hashin Z. Thermoelastic properties of particulate composites with imperfect interface. J Mech Phys Solids 1991;39:745–62.
[17] Hashin Z, Rosen BW. The elastic moduli of fiber-reinforced materials. J Appl Mech 1964;31:223–32.
[18] Ju JW, Chen TM. Micromechanics and effective moduli of elastic composites containing randomly dispersed ellipsoidal inhomogeneities. Acta Mech 1994;103:103–21.
[19] Ju JW, Chen TM. Effective elastic moduli of two-phase composites containing randomly dispersed spherical inhomogeneities. Acta Mech 1994;103:123–44.
[20] Ju JW, Lee HK. A micromechanical damage model for effective elastoplastic behavior of ductile matrix composites considering evolutionary complete particle debonding. Comput Methods Appl Mech Eng 2000;183:201–22.
[21] Ju JW, Lee HK. Micromechanical damage model for effective elastoplastic behavior of partially debonded ductile matrix composites. Int J Solids Struct 2001;38:6307–32.
[22] Ju JW, Sun LZ. Effective elastoplastic behavior of metal matrix composites containing randomly located aligned spheroidal inhomogeneities. Part I: micromechanics-based formulation. Int J Solids Struct 2001;38:183–201.

[23] Kim BR, Lee HK. Modeling of particle debonding and void evolution in particulate ductile matrix composites. CMES: Comput Model Eng Sci 2009;47:253–81.
[24] Lakes R. Viscoelastic materials. Cambridge: Cambridge University Press; 2009.
[25] Lee HK. A computational approach to the investigation of impact damage evolution in discontinuously reinforced fiber composites. Comput Mech 2001;27:504–12.
[26] Lee HK, Hausmann LR. Structural repair and strengthening of damaged RC beams with sprayed FRP. Compos Struct 2004;63:201–9.
[27] Lee HK, Pyo SH. Micromechanics-based elastic damage modeling of particulate composites with weakened interfaces. Int J Solids Struct 2007;44:459–74.
[28] Lee HK, Pyo SH. An elastoplastic multi-level damage model for ductile matrix composites considering evolutionary weakened interface. Int J Solids Struct 2008;45:1614–31.
[29] Lee HK, Pyo SH. Multi-level modeling of effective elastic behavior and progressive weakened interface in particulate composites. Compos Sci Technol 2008;68:387–97.
[30] Lee HK, Simunovic S. Modeling of progressive damage in aligned and randomly oriented discontinuous fiber polymer matrix composites. Compos Part B: Eng 2000;31:77–86.
[31] Lee HK, Simunovic S. A damage constitutive model of progressive debonding in aligned discontinuous fiber composites. Compos Part B: Eng 2001;38:875–95.
[32] Lee HK, Simunovic S, Shin DK. A computational approach for prediction of the damage evolution and crushing behavior of chopped random fiber composites. Comp Mater Sci 2004;29:459–74.
[33] Liang Z, Lee HK, Suaris W. Micromechanics-based constitutive modelling for unidiretional laminated composites. Int J Solids Struct 2006;43:5674–89.
[34] Li J, Weng GJ. Strain-rate sensitivity, relaxation behavior, and complex moduli of a class of isotropic viscoelastic composites. J Eng Mater Technol 1994;116:495–504.
[35] Li J, Weng GJ. Effect of a viscoelastic interphase on the creep and stress/strain behavior of fiber-reinforced polymer matrix composites. Compos Part B: Eng 1996;27:589–98.
[36] Marzari N, Ferrari M. Textural and micromorphological effects on the overall elastic response of macroscopically anisotropic composites. J Appl Mech 1992;59:269–75.
[37] Matzenmiller A, Gerlach S. Micromechanical modeling of viscoelastic composites with compliant fiber-matrix bonding. Comput Mater Sci 2004;29:283–300.
[38] McCrum NG, Buckley CP, Bucknall CB. Principles of polymer engineering. Oxford University Press; 1997.
[39] Meraghni F, Benzeggagh ML. Micromechanical modeling of matrix degradation in randomly discontinuous-fibre composites. Compos Sci Technol 1995;55:171–86.
[40] Odegard GM, Gates TS, Wise KE, Park C, Siochi EJ. Constitutive modeling of nanotube-reinforced polymer composites. Compos Sci Technol 2003;63:1671–87.
[41] Pan HH, Weng GJ. Study on strain-rate sensitivity of cementitious composite. J Eng Mech 2010;136:1076–82.
[42] Plaseied A, Fatemi A. Deformation response and constitutive modeling of vinyl ester polymer including strain rate and temperature effects. J Mater Sci 2008;43:1191–9.
[43] Pyo SH, Lee HK. Micromechanical analysis of aligned and randomly oriented whisker-/short fiber-reinforced composites. CMES: Comput Model Eng Sci 2009;40:271–306.
[44] Rikards R, Chate A, Bliedzki AK, Kushnevsky V. Numerical modeling of damping properties of laminated composite. Mech Compos Mater 1994;30:359–71.
[45] Schapery RA. On the characterization of nonlinear viscoelastic materials. Polym Eng Sci 1969;9:295–310.
[46] Shen W, Peng L, Yue Y. Damage-dependent viscoelastic constitutive relations for glass–fiber woven/polyester composite plate. Eng Fract Mech 1994;47:867–72.
[47] Simo JC. On a fully three-dimensional finite-strain viscoelastic damage model: formulation and computational aspects. Comput Methods Appl Mech Eng 1987;60:153–73.
[48] Sun LZ, Ju JW. Elastoplastic modeling of metal matrix composites containing randomly located and oriented spheroidal particles. J Appl Mech 2004;71:774–85.
[49] Tohgo K, Weng GJ. A progress damage mechanics in particle-reinforced metal–matrix composites under high triaxial tension. ASME J Eng Mater Technol 1994;116:414–20.
[50] Vidal-Sallé E, Chassagne P. Constitutive equations for orthotropic nonlinear viscoelastic behaviour using a generalized maxwell model application to wood material. Mech Time-Depend Mater 2007;11:127–42.
[51] Wang W, Makarov G, Shenoi RA. An analytical model for assessing strain rate sensitivity of unidirectional composite laminates. Compos Struct 2005;69:45–54.
[52] Weibull W. A statistical distribution function of wide applicability. J Appl Mech 1951;18:293–7.
[53] Zhang Y, Xia Z, Ellyin F. Nonlinear viscoelastic micromechanical analysis of fibre-reinforced polymer laminates with damage evolution. Int J Solids Struct 2005;42:591–604.
[54] Zhao YH, Weng GJ. A theory of inclusion debonding and its influence on the stress-stain relations of a ductile matrix. Int J Damage Mech 1995;4:196–211.
[55] Zhao YH, Weng GJ. Plasticity of a two-phase composite with partially debonded inclusions. Int J Plast 1996;12:781–804.
[56] Zhao YH, Weng GJ. Transversely isotropic moduli of two partially debonded composites. Int J Solids Struct 1997;34:493–507.